

Formation of Titanium Nitride, Titanium Carbide, and Silicon Carbide Surfaces by High Power Femtosecond Laser Treatment

Rostislav Fedorov,^[a] Felix Lederle,^[a] Mingji Li,^[a] Vinzent Olszok,^[b] Karl Wöbbing,^[a] Wolfgang Schade,^[a, c] and Eike G. Hübner*^[a, d]

Coatings based on titanium nitrides, titanium carbides and silicon carbides can optimize the surface properties of titanium or silicon for various applications ranging from biocompatibility to chemical stability and durability. Here, we investigated a high power (100 W) high pulse repetition rate femtosecond laser process ($\lambda = 1030$ nm, $\tau = 750$ fs, $f = 1$ MHz) for the treatment of titanium and silicon in atmospheres of argon, nitrogen, methane, ethene and acetylene. In a nitrogen atmosphere, a homogeneous coating of TiON is formed on titanium. In an

ethene/argon atmosphere coatings of TiOC and SiC are formed on Ti and Si, respectively. The process allows a fast surface transformation with a process rate of 0.33 cm²s⁻¹ and a high spatial resolution below 0.5 mm with a minimal heat affected zone at the same time. In contrast to low repetition rate femtosecond laser processed samples, the surfaces are more robust against mechanical impact. At the same time, the surfaces reveal a distinct microstructure in comparison to coatings obtained by vapor deposition techniques.

Introduction

Surface coating of titanium and silicon with a layer of the corresponding and highly stable titanium nitride/oxynitride, titanium carbide or silicon carbide, respectively, is of great interest for various applications. SiC is an extremely hard material, stable in chemically aggressive and radiative environments. TiC and TiN as comparably hard materials provide excellent surface properties such as corrosion and wear resistance.^[1–3] Titanium nitride/oxynitride are of special interest due to their biocompatibility, ability to osseointegrate and prevent hyperplasia and therefore used as coatings for medical implants and stents.^[4–6] Typically, these coatings are achieved

by reactive gas sputtering of pure titanium in nitrogen/nitrogen + oxygen atmospheres (TiON), chemical vapor deposition by thermal decomposition of precursors such as hexamethyldisilane (SiC) or by chemical processes directly on the surfaces, e.g. plasma induced in a methane atmosphere on silicon (SiC) or on titanium in the presence of nitrogen/oxygen (TiON).^[1–5,7,8] Instead of a plasma source to promote surface reaction or film deposition, ultrashort laser pulses can be used to initiate a plasma plume on the surface. Detailed investigations and reviews compare and evaluate the application of continuous wave/millisecond (mainly Nd:YAG and CO₂), nanosecond (mainly Nd:YAG and excimer (UV)) and free electron laser sources for laser nitriding in the presence of nitrogen and carburizing typically in the presence of methane.^[9–12]


Femtosecond (fs) lasers, operating on an extremely short timescale with pulses of some 10^{-14} s, are usually used to form unique surface structures with tunable properties.^[13,14] Femtosecond lasers have been applied to tailor the surface properties of the ultrahard materials such as titanium nitride, titanium carbides and silicon carbide as well as thin films thereof.^[15–21] In these cases, laser induced periodic surface structures (LIPSS) in form of parallel lines at a periodicity roughly at the wavelength of the incident laser beam are an important structural motif formed on the surface.^[16–18,20,22] The resulting surfaces can improve tribological properties, reduce friction or enhance biocompatibility.^[16,17,20] Besides the post-processing of deposited or bulk material, femtosecond laser have been applied to synthesize and/or deposit nanoparticles and films of nitrides or carbides, respectively, on substrates. The direct material transfer has been realized by femtosecond laser treatment of targets from SiC or TiC and deposition of the ablated material on silicon and other substrates.^[23,24] SiC nanoparticles have been obtained with femtosecond laser irradiation of silicon immersed in hexane or ethanol, respectively.^[25,26] A similar process has been


[a] R. Fedorov, F. Lederle, M. Li, K. Wöbbing, Prof. Dr. W. Schade, Apl. Prof. Dr. E. G. Hübner
Fraunhofer Heinrich Hertz Institute HHI
Fiber Optical Sensor Systems
Am Stollen 19 H, 38640 Goslar (Germany)
E-mail: eike.huebner@tu-clausthal.de

[b] V. Olszok
Clausthal University of Technology
Institute of Particle Technology
Leibnizstr. 19, 38678 Clausthal-Zellerfeld (Germany)

[c] Prof. Dr. W. Schade
Clausthal University of Technology
Institute of Energy Research and Physical Technologies
Am Stollen 19 B, 38640 Goslar (Germany)

[d] Apl. Prof. Dr. E. G. Hübner
Clausthal University of Technology
Institute of Organic Chemistry
Leibnizstr. 6, 38678 Clausthal-Zellerfeld (Germany)

 Supporting information for this article is available on the WWW under <https://doi.org/10.1002/cplu.202100118>

 © 2021 The Authors. ChemPlusChem published by Wiley-VCH GmbH. This is an open access article under the terms of the Creative Commons Attribution Non-Commercial NoDerivs License, which permits use and distribution in any medium, provided the original work is properly cited, the use is non-commercial and no modifications or adaptations are made.

applied on titanium immersed in hexane for the synthesis of TiC microparticles.^[27] Longer pulses have been used to ablate titanium in a methane atmosphere and to deposit the resulting TiC as a film on silicon targets.^[28] Films of TiN on silicon have been achieved by femtosecond laser treatment of titanium targets in a nitrogen atmosphere.^[29] The direct surface transformation of Ti and Si to their corresponding nitrides or carbides with femtosecond laser pulses has been investigated, too. A silicon surface coated with carbon is transformed to SiC by femtosecond laser irradiation.^[30] A TiC surface is formed on Ti plates immersed in hexane or acetone upon femtosecond laser pulse treatment.^[31–33] A TiN/TiON surface is formed on titanium by femtosecond laser pulses in a nitrogen atmosphere.^[34,35] Cleaning the surface with a first femtosecond laser process in argon leads to a pure Ti surface, on which TiN is formed in a second step under N₂ atmosphere.^[35] In liquid nitrogen, TiN is formed upon femtosecond laser irradiation of titanium, too, and the surface is covered with an inhomogeneous, cracked TiN layer.^[32]

The nitride and carbide surfaces achieved by reactive femtosecond laser treatment with typically Ti:sapphire laser setups have been compared in detail to surfaces achieved by nanosecond lasers or other methods in literature and reveal a significant drawback of the femtosecond process.^[9,10,12] Despite the nicely structured surface with a high specific surface area,

the surface is rather porous and the hardness of the surface is strongly reduced in comparison to the bare metal.^[9,10,12] Consequently, the surface layer is easily scratched off. This is explained by the short interaction time of the laser beam and direct ablation of the nitrated material instead of melting processes on the surface which facilitate a strong binding of the surface layer with the substrate.^[12] This situation is visualized in Figure 1. A titanium sample has been laser structured with femtosecond laser pulses from a Ti:sapphire setup in a nitrogen atmosphere. The EDX measurements confirm a nitrogen content of approx. 18 atom-% on the surface. Weakly scratching the surface with a hardness pick of Mohs hardness 5, i.e. below the hardness of blank titanium (see Table 1), completely removes the structured surface coating and the bare metal appears.

Here, we investigated the surface treatment of titanium and silicon in a nitrogen atmosphere or in the presence of gaseous carbon sources such as methane, ethylene and acetylene with femtosecond laser pulses from a high power laser setup with high repetition rates. High power fast pulse repetition rate femtosecond lasers fill the gap between lower repetition rate femtosecond laser sources and nanosecond laser treatment. We report on a stable carbide or nitride layer formed with a processing time of a few seconds per square centimeter and an excellent spatial resolution below 1 mm.

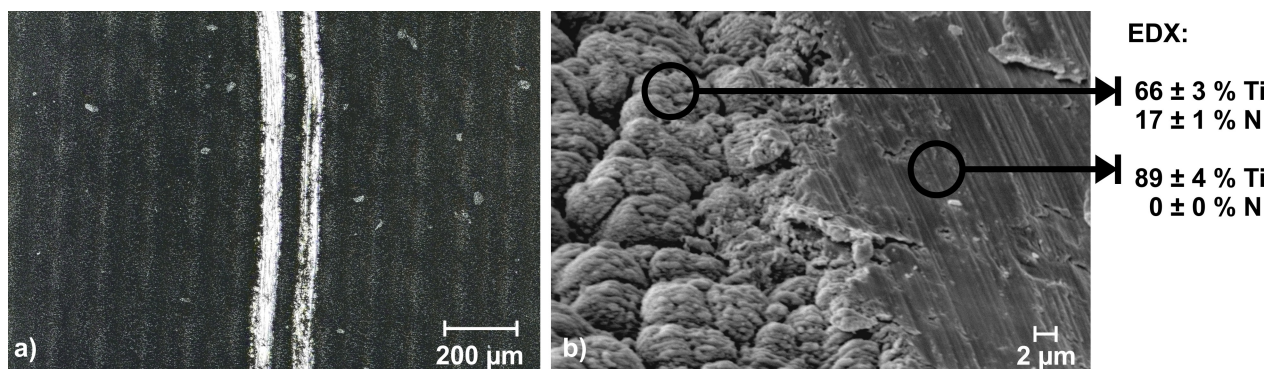


Figure 1. Titanium surface treated with fs laser pulses of a Ti:sapphire laser source ($\tau = 60$ fs, $f = 10$ kHz, $J = 1.44$ J cm⁻², $N = 250$, $S_{\text{spot}} = 140$ μm, $D_{\text{line}} = 60$ μm, N₂ atmosphere) scratched with a tip of Mohs hardness 5. (a) Optical microscopic image and (b) close-up view by SEM with surface composition obtained from EDX measurements.

Table 1. Physical properties of the metal targets, the reagents and reaction products discussed here.

	m.p. ^[41] [°C]	b.p. ^[41] [°C]	heat of formation $\Delta_f H^\circ$ [kJ/mol]	Mohs hardness
Ti	1668	3287	0	6.0 ^[42]
Ti6Al4V	1655 ^[44]			
Si	1414	3265	0	6.5 ^[42]
TiO ₂	1843	~3000 ^[45]	-944.8 ^[48]	6.2 ^[41]
TiN	2950 (dec.)	-	-338 ^[49]	9.0 ^[41]
TiC	3067	4820 ^[47]	-193.3 ^[50]	9 ^[41a,43]
SiC	2830 (dec.)	-	-65.3 ^[46]	9.3 ^[41]
N ₂	-210.0	-198.8	0	-
CH ₄	-182.5 ^[46]	-161.5 ^[46]	-74.9 ^[46]	-
ethene	-169 ^[46]	-104 ^[46]	+52.1 ^[46]	-
ethyne	-81 ^[46]	-84 ^[46]	+226.9 ^[46]	-

[a] estimated from Knoop's hardness.

Results and Discussion

For all experiments, a vacuum-tight stainless steel chamber with a glass window, pressure and oxygen sensors as well as a gas-mixing inlet has been used (Figure 2). The chamber is placed on a water cooled baseplate ($T=15^{\circ}\text{C}$). An Yb:YAG laser with a center wavelength of $\lambda=1030\text{ nm}$ and a pulse length of $\tau=750\text{ fs}$ with a maximum output power of $P=400\text{ W}$ at repetition rate of $f=1\text{ MHz}$ has been applied as beam source. The laser beam has been scanned in parallel lines across the surface. Laser parameters for surface treatment have been derived from the parameters of a Ti:sapphire laser setup for titanium.^[36] The resulting surface structure achieved with the Ti:sapphire setup is visualized in Figure 1. In perfect agreement with literature, the fluence of $J=1.44\text{ Jcm}^{-2}$ and a number of repetitive laser pulses of $N=250$ on each spot of the surface leads to a microconical structure on the titanium sample.^[37,38] Transferring the parameters to our high power setup with 1 MHz repetition rate at an average output power of $P=222\text{ W}$ leads to a very fast structuring process. Owing to incubative effects, surface structures differ strongly and structure formation is absent. Instead, molten grooves located at the parallel lines of the focus spot moving across the surface are observed.^[37] Depending on the repetition rate, different structure formation processes are dominating, and high pulse repetition rate laser systems form other structural motifs on the surface with matching laser parameter sets.^[39,40] The limits are roughly characterized around $f<250\text{ kHz}$; $250\text{ kHz}-5\text{ MHz}$; $5-7\text{ MHz}$; $>7\text{ MHz}$.^[40] Here, we reduced the laser fluence until the occurrence of molten/milled grooves was absent to ensure a homogeneous surface. This was achieved at a fluence of $J=0.62\text{ Jcm}^{-2}$. The final laser parameters used for all samples presented here are a spot size of $S_{\text{spot}}=140\text{ }\mu\text{m}$, a number of pulses of $N=250$ per spot on the surface, a resulting processing speed of 560 mms^{-1} and a distance of the laser processed lines of $D_{\text{line}}=60\text{ }\mu\text{m}$.

The line distance is lower than the spot radius, which again supports formation of a homogeneous surface (see below for a variation of the line distance). The applied laser fluence of $J=0.62\text{ Jcm}^{-2}$ is clearly above the ablation threshold on titanium of $J=0.1\text{ Jcm}^{-2}$.^[51] On silicon, the laser fluence was slightly reduced to $J=0.50\text{ Jcm}^{-2}$ to prevent cracks on the surface. On silicon, the ablation threshold is strongly wavelength dependent. Owing to the increased transparency at 1030 nm ,^[52] the laser beam can penetrate deeper into the material. Here, the applied fluence is clearly above the documented ablation threshold on silicon at 1030 nm of $J=0.4\text{ Jcm}^{-2}$.^[53]

Based on the line distance and the processing speed, a sample of $1\times 1\text{ cm}^2$ takes 3 s to process. For the given fluence of $J=0.62\text{ Jcm}^{-2}$ on Ti, the laser is operated at $P=95\text{ W}$. As a rough estimation, the bulk material of the Ti samples of 0.5 mm thickness could easily reach a temperature above the melting point of Ti if the energy is transferred in the sample. Since the structuring process was strictly limited to the scanned area (see below), it can be assumed that despite the fast process time only surface reactions are dominant.

The properties of all samples are summarized in Table 2. First, the metal plates have been processed in an argon atmosphere for comparison. After processing, the surface of the titanium sample Ti-Ar appears as a homogeneously roughened, shiny surface (Figure 3a). The visible roughness is reflected by laser scanning microscopy (LSM) which reveals an increase of the surface roughness in comparison to the untreated plate from $R_a=0.5\pm 0.1\text{ }\mu\text{m}$ to $2.2\pm 0.1\text{ }\mu\text{m}$. The reflectivity of the surface is slightly reduced by the roughening process and the absorptivity is increased from $\alpha=65\%$ to 77% . The homogeneous surface structure on a microscopic level is confirmed by light microscopic images. The titanium sample processed under argon shows a microscopically regular structured motif (Figure 4a). Basically the same observation has been made for the silicon sample Si-Ar. The smooth surface ($R_a=0.11\pm 0.01\text{ }\mu\text{m}$) is roughened after processing ($R_a=2.3\pm 0.7\text{ }\mu\text{m}$)

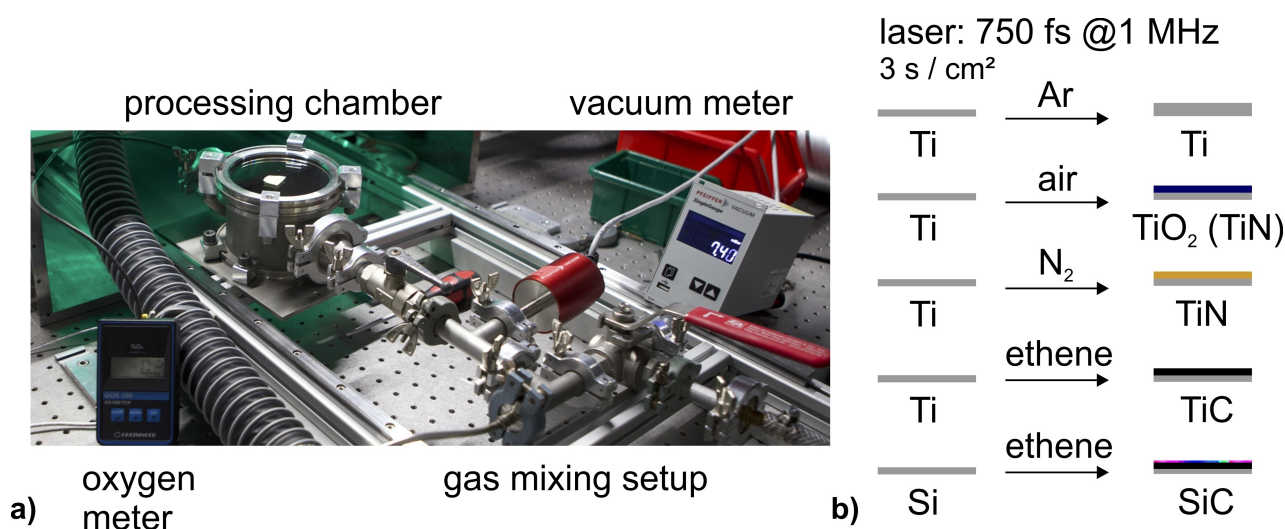


Figure 2. (a) Process chamber for irradiation of the samples under various controlled gas atmospheres and (b) sketch of the surface chemistry on titanium and silicon upon high repetition rate femtosecond laser treatment.

Table 2. Properties of the surfaces treated with 750 fs/1 MHz laser pulses in various atmospheres.						
sample	atmosphere	surface composition ^[a] [atom-%]			surface roughness ^[b] R_a [μm]	absorptivity ^[c] α [%]
		O	N	C		
Ti	untreated	12.7 ± 1.0	–	4.7 ± 0.3	0.5 ± 0.1	65
Ti6Al4V	untreated	21.0 ± 1.6	–	6.2 ± 0.4	0.6 ± 0.1	67
Si	untreated	0.4 ± 0.1	–	6.9 ± 0.9	0.11 ± 0.01	69
Ti-ref ^[d]	N_2	12.7 ± 1.0	16.8 ± 1.0	4.2 ± 0.3	3.1 ± 0.1	98
Ti-Ar	argon	14.8 ± 1.2	–	4.8 ± 0.3	2.2 ± 0.1	77
Ti-air	air	53.7 ± 4.2	3.5 ± 0.4	2.8 ± 0.3	3.1 ± 0.1	89
Ti6Al4V-air	air	54.4 ± 4.5	3.0 ± 0.3	3.7 ± 0.4	5.6 ± 0.3	–
Ti-N	N_2	14.7 ± 1.3	20.3 ± 1.3	5.8 ± 0.4	2.0 ± 0.1	85
Ti6Al4V-N	N_2	16.2 ± 1.3	18.2 ± 1.1	6.0 ± 0.4	2.9 ± 0.1	–
Ti6Al4V-C	methane	17.3 ± 1.1	–	22.9 ± 2.0	–	–
	ethene/Ar 60/40	12.4 ± 2.4	–	30.6 ± 2.6	2.9 ± 0.1	–
	ethyne/Ar 20/80	14.3 ± 0.9	–	17.9 ± 1.7	–	–
TiC	ethene/Ar 60/40	7.3 ± 1.5	–	28.1 ± 2.2	2.9 ± 0.1	94
Si-Ar	argon	0.8 ± 0.2	–	9.2 ± 1.1	2.3 ± 0.7	70
Si-C	ethene/Ar 60/40	2.1 ± 0.4	–	19.6 ± 2.0	2.2 ± 0.3	80

[a] measured by EDX. [b] measured by LSM. [c] at 600 nm. [d] processed with a Ti:sapphire laser setup and 60 fs/10 kHz pulses.

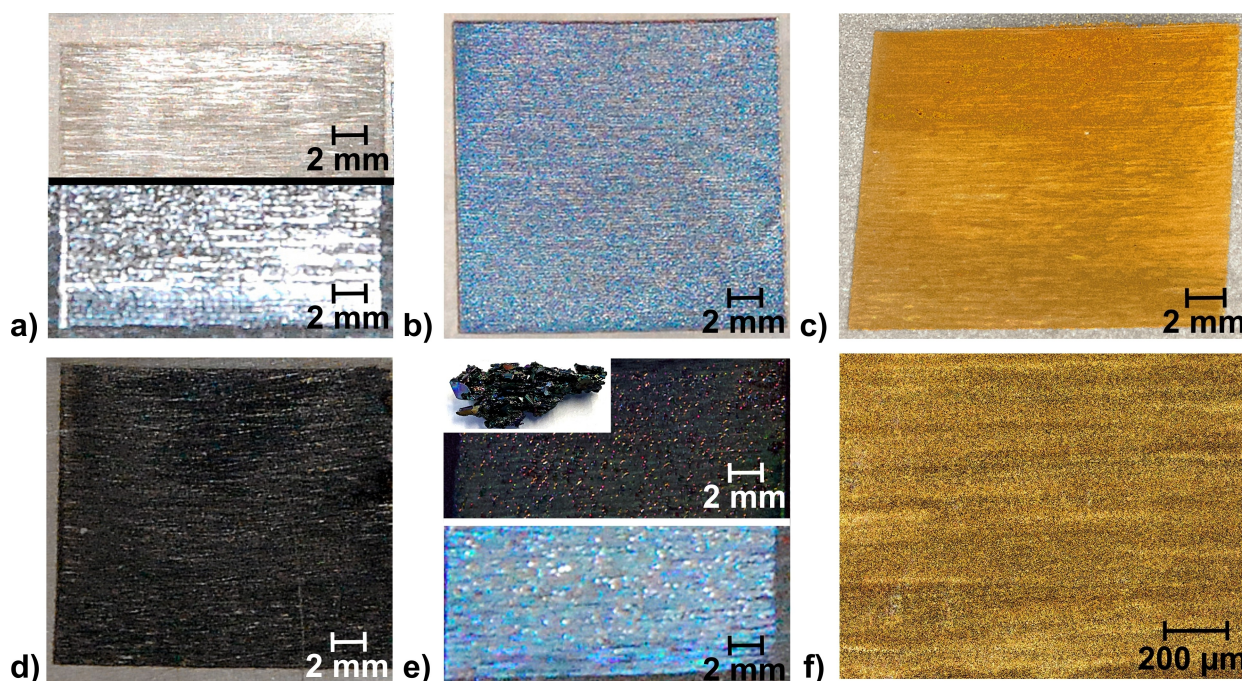


Figure 3. Photographic images of surfaces treated with high repetition rate fs laser pulses ($\tau = 750$ fs, $f = 1$ MHz, $N = 250$, $S_{\text{spot}} = 140$ μm , $D_{\text{line}} = 60$ μm , $J = 0.62$ J cm^{-2} (Si: $J = 0.50$ J cm^{-2}). (a) Ti (top) and Si (bottom) treated in Ar, (b) Ti in air, (c) Ti in N_2 , (d) Ti in ethene/argon atmosphere (top at ambient light, bottom with flashlight), insert: commercial SiC crystals. (f) Optical microscopic image of the Ti sample treated under N_2 atmosphere.

and visibly comparable to the titanium sample (Figure 3a). According to the elemental surface analysis by energy dispersive X-ray spectroscopy (EDX), the chemical surface composition remains unchanged during the structuring process. The titanium surface provides a significant oxygen content before structuring (12.7 ± 1.0 atom-% O) which is not removed with the laser process applied here after laser structuring in an argon atmosphere.

Processing titanium at air, reveals a significantly different surface. The surface of **Ti-air** appears periodically roughened and inhomogeneously colored. The sample appears in a blue color, with an increased absorptivity of $\alpha = 89\%$, indicating the

formation of oxygen-deficient TiO_2 , with golden spots or lines in between (Figure 3b). EDX measurements confirm a high oxygen content of $53.7 \pm 4.2\%$. Additionally, a significant amount of nitrogen (3.5 ± 0.4 atom-% N) is detected. The surface inhomogeneity is visualized by optical micrographs (Figure 4). In contrast to the homogeneously structured surface after laser processing in an argon atmosphere (Figure 4a), large grooves after laser processing at air dominate the surface (Figure 4b). This is reflected by the increased roughness of $R_a = 3.1 \pm 0.1$ μm of the sample **Ti-air**. The formation of the deep grooves is explained by etching processes of highly reactive oxygen, which dominate the structuring process.^[36,54]

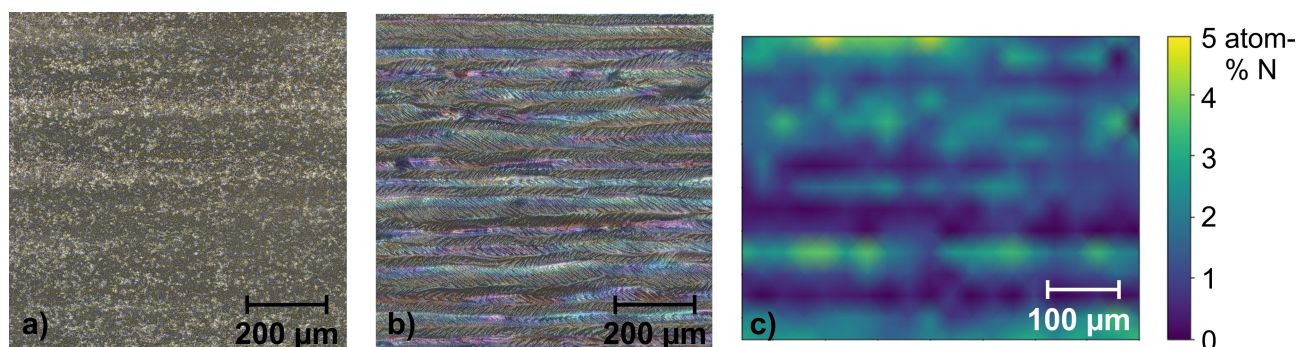


Figure 4. Optical microscopic images of titanium samples treated under (a) an argon atmosphere and (b) at air. (c) Elemental distribution map for the nitrogen content obtained by EDX for the sample Ti-air.

Interestingly, the color of the parallel lines is alternating blue and golden (Figure 4b). To further analyze the chemical composition, spatially resolved EDX measurements were performed. The elemental composition map reveals alternating lines of 4–5 atom-% N and 0% N at a periodicity of the line distance of the laser process. Consequently, we assume at the center of the laser spot oxygen to be consumed fastest and subsequently titanium to react with the less reactive nitrogen (heat of formation $\Delta_f H^0 = -945 \text{ kJ mol}^{-1}$ for TiO_2 and -338 kJ mol^{-1} for TiN), while at the outer area of the gaussian beam profile the reaction is slower and sufficient oxygen is present to form solely titanium oxide. The oxygen concentration is randomly distributed across the surface with a slight increase at the areas with the highest nitrogen content (see Figure S1 of the Supporting Information). The experiments have been repeated in a pure oxygen atmosphere to obtain a surface free of TiN, but the reactivity of Ti in oxygen turned out to be too high and the sample ignited upon high power laser irradiation and was burned (see Figure S3 of the Supporting Information).

In a nitrogen atmosphere, laser structuring proceeded well and a homogeneous, deep golden surface was obtained (Figure 3c). The visible surface structure of Ti-N matches with the sample processed under argon. The microscopic images (Figure 3f) demonstrate the homogeneous golden coating on the titanium sample, with a roughening already seen in the microscopic image of Ti-Ar (Figure 4a). The measured surface roughness of $R_a = 2.0 \pm 0.1 \mu\text{m}$ is in agreement with Ti-Ar, too. The nitrogen content of Ti-N is determined to $20.3 \pm 1.3 \text{ atom-% N}$, which is slightly above the residual oxygen content. Consequently, we assume titanium oxynitride to be formed (see below) roughly with a N:O ratio of 1:0.75. This is especially of interest concerning the surface hardness. Titanium oxynitrides provide a constant hardness from an N/O fraction of 1/0 to 0.3/0.7, while at lower nitrogen contents the hardness suddenly drops off to the hardness of TiO_2 .^[4] The golden color of the sample differs strongly from the black surface obtained with the Ti:sapphire laser setup with a repetition rate of 10 kHz (Ti-ref). This reflected by the absorptivity of $\alpha = 85\%$ for Ti-N in comparison to 98% for Ti-ref. The porous microcones of Ti-ref act as light trap, while in case of Ti-N surface chemistry and not

the surface structure dominates the visible appearance. The line distance of the laser structuring process has been reduced from $D_{\text{line}} = 60 \mu\text{m}$ gradually to $3 \mu\text{m}$ to investigate if surface functionalization can be increased, but with decreasing line distance the surfaces became inhomogeneous and heat accumulation led to destroyed areas (see Figure S5 of the Supporting Information).

All experiments have been repeated with Ti-6Al-4V as important titanium alloy for industrial and medical use. For an application, the surface coating is more likely to be applied on alloys such as Ti-6Al-4V instead of pure titanium. Fortunately, nearly identical results for the surface structuring process for the samples processed under a nitrogen atmosphere (and at air) have been obtained in terms of the optical appearance, surface roughness and elemental composition. The results are summarized in Table 2 in detail.

Since the incorporation of nitrogen worked well, the formation of TiC on Ti-6Al-4V was investigated next. Methane was applied as gaseous carbon source to avoid cooling mechanisms of a liquid medium, which could favor particle release and prevent a stable binding of the surface layer on the bulk material. After laser processing in a pure methane atmosphere, the surface showed an inhomogeneous, partly black partly silvery appearance (see Figure S6a of the Supporting Information). Although EDX measurements reveal a carbon content of $22.9 \pm 2.0 \text{ atom-% C}$, the surface is not uniformly transformed. The surface structure, visibly just between the structuring process achieved under argon with black parts, may be explained by partial carbon release from methane and partially methane acting as inert gas. To facilitate the release of carbon from the gas atmosphere, ethyne was applied as reactive gas. As endothermic compound ($\Delta_f H^0 = 226.9 \text{ kJ mol}^{-1}$ in comparison to methane $\Delta_f H^0 = -74.9 \text{ kJ mol}^{-1}$) ethyne readily decomposes under the release of carbon. The formation of elemental carbon can be seen as advantageous, since the transformation of a Ti sample to TiC by laser structuring the Ti surface after a layer of pure carbon had been deposited has been demonstrated in literature.^[30] Ethyne has been used as carbon source for the synthesis of TiC nanoparticles from SiH_4 by laser pyrolysis.^[55] Since ethyne/oxygen mixtures can explode even if highly diluted with inert argon and furthermore pure

ethyne can violently decompose, careful control of the gas mixture is required.^[56] We gradually increased the ethyne content beginning with 5 vol-% ethyne up to 21 vol-% of ethyne in Ar. Above 21 vol-% the carbon release was too intense and the chamber got filled with black dust. The glass window of the chamber is a critical point for carbon formation and above 21 vol-% of ethyne the chamber window becomes coated with a layer of carbon and molten glass at the entry point of the incident laser beam (see Figure S4 of the Supporting Information for an image of 1 x 1 cm² structured area of the glass window). The sample did not incorporate more carbon than the sample processed in a methane atmosphere. Although the surface appears darker, the carbon content determined by EDX is not increased in comparison to the sample processed in methane (see Table 2) and the surface is still inhomogeneous (see Figure S6b of the Supporting Information). Finally, ethene was applied as reactive gas. Ethene is still endothermic ($\Delta_f H^\circ = 52.1 \text{ kJ mol}^{-1}$) but significantly more stable than ethyne. Again, ethene was diluted with argon and the ethene content was gradually increased. Up to 60 vol-% of ethene the structuring process worked reproducibly without damaging the chamber window and with only slight formation of dusty carbon. The sample processed in a 60/40 mixture of ethene/argon revealed a strongly increased carbon content of $30.6 \pm 2.6 \text{ atom-\% C}$ and a deep black appearance. The experiments could be repeated on pure titanium with the same results. The visible image of Ti-C demonstrates the homogeneous black surface (Figure 3d) with a weak, regular underlying rough structure ($R_a = 2.9 \pm 0.1$) comparable to Ti-N. The absorptivity of Ti-C is increased to $\alpha = 94\%$ in accordance with the black appearance. The oxygen content of the samples is reduced to $7.3 \pm 1.5 \text{ atom-\% O}$ in comparison to the samples processed under nitrogen and the untreated Ti surface (see Table 2), which can be explained by a reaction of incorporated oxygen with hydrogen released during the decomposition of ethene.

These optimized conditions have been applied to treat a silicon sample. Although the wavelength of $\lambda = 1030 \text{ nm}$ is not optimal for the structuring process of Si,^[52] a significantly roughened surface was obtained after laser processing the Si sample in pure argon (Figure 3a). The surface roughness is comparable to the Ti samples (Table 2). Repeating the experiment within the ethene/argon 60/40 atmosphere led to a dark, colorful glittering surface (Figure 3e). The visual appearance of Si-C reminds to the typical black crystals of SiC iridescenting in all colors. The carbon content is determined to $19.6 \pm 2.0 \text{ atom-\% C}$ indicating a less effective process than on TiC. Partly, this may be explained by the less favored product formation ($\Delta_f H^\circ = -65.3 \text{ kJ mol}^{-1}$ for SiC). The roughness of the surface processed in the presence of ethene is comparable to the structuring process under pure argon. To evaluate the surface morphology in detail, SEM images have been taken of all samples (Figure 5). The titanium samples obtained in argon, nitrogen and ethene/argon atmosphere reveal basically the same microstructure (Figure 5a,d,f). The surface is roughened in comparison to the plane metal, but the formation of microcones or deeper structures is absent. Laser induced periodic surface structures

(LIPSS) have been detected in all these cases as a weak substructure (see insert in Figure 5a,d,f). Low spatial frequency LIPSS, formed perpendicular to the polarization of the incident beam and consequently perpendicular to the scanning direction, here, are a typical substructure of the laser process. These LIPSS are formed due to interference of incident laser light with electromagnetic waves formed on the irradiated and excited surface.^[57] The periodicity is usually slightly below the wavelength of the incident beam and has been measured to approx. 700 nm. The periodicity matches well with the expected distance given in literature for LIPSS formed on Ti by 1030 nm irradiation.^[57] The surface structure of the sample processed at air differs strongly. Wavy structures in form of parallel grooves formed in scanning direction appear on the surface (Figure 5b). LIPSS have not been observed on the samples processed at air. This observation is in contrast to results concerning the formation of LIPSS on Ti by laser treatment at air presented in literature^[57] and can be explained by the high power laser source used here, with a longer pulse length and a higher repetition rate. On the high power setup, etching processes dominate the structuring process in the presence of oxygen.^[36] A fine porous network is formed as substructure on the large grooves (Figure 5c). The grooves are oriented at a distance, which is smaller than the distance of the laser processed lines. The grooves are built up alternately with a shorter and a longer spacing, which is in accordance with literature. An explanation is given by a U shaped substructure caused by faults on the sides of a groove^[58] and additionally by an offset of 10 μm of the size of the laser spot ($R_{\text{spot}} = 70 \mu\text{m}$) to the line distance ($D_{\text{line}} = 60 \mu\text{m}$). On silicon, laser processing leads to a unique surface structure based on thin tiles or scales with a dimension of approx. $100 \times 200 \mu\text{m}^2$ regularly formed on the whole surface (Figure 5g). Possibly, the tiles are formed due to thermal stress on the silicon surface. These microscales explain the surface roughness discussed above. Every scale itself provides a flat surface (Figure 5h). The situation changes in presence of ethene. The silicon sample processed in an ethene/argon 60/40 atmosphere reveals comparable tiles, but the surface of every tile is covered with a substructure of LIPSS with a periodicity of approx. 800 nm (Figure 5i). The structure on each scale looks similar to the titanium surface discussed above. Overall, the SEM images reveal the surfaces on titanium and on silicon to be clearly structured in comparison to the blank material, but with comparably solid structures, i.e. LIPSS in contrast to porous microcones of the laser structuring process with 10 kHz repetition rate are formed.

The transition of the unstructured to the structured area is sharp (Figure 5e) and despite the high repetition rate a heat affected zone (HAZ) neighbored to the structured area is not visible. This is an advantage of a femtosecond laser based process as long as heat accumulation due to incubative effects remains absent. Consequently, the surface transformation of more complex geometries was investigated. Figure 6 shows the formation of titanium carbide on Ti-6Al-4V by laser scanning a vector image with the laser parameter set discussed above on the Ti surface under an ethene/argon 60/40 atmosphere. Fortunately, surface transformation worked well and fine lines

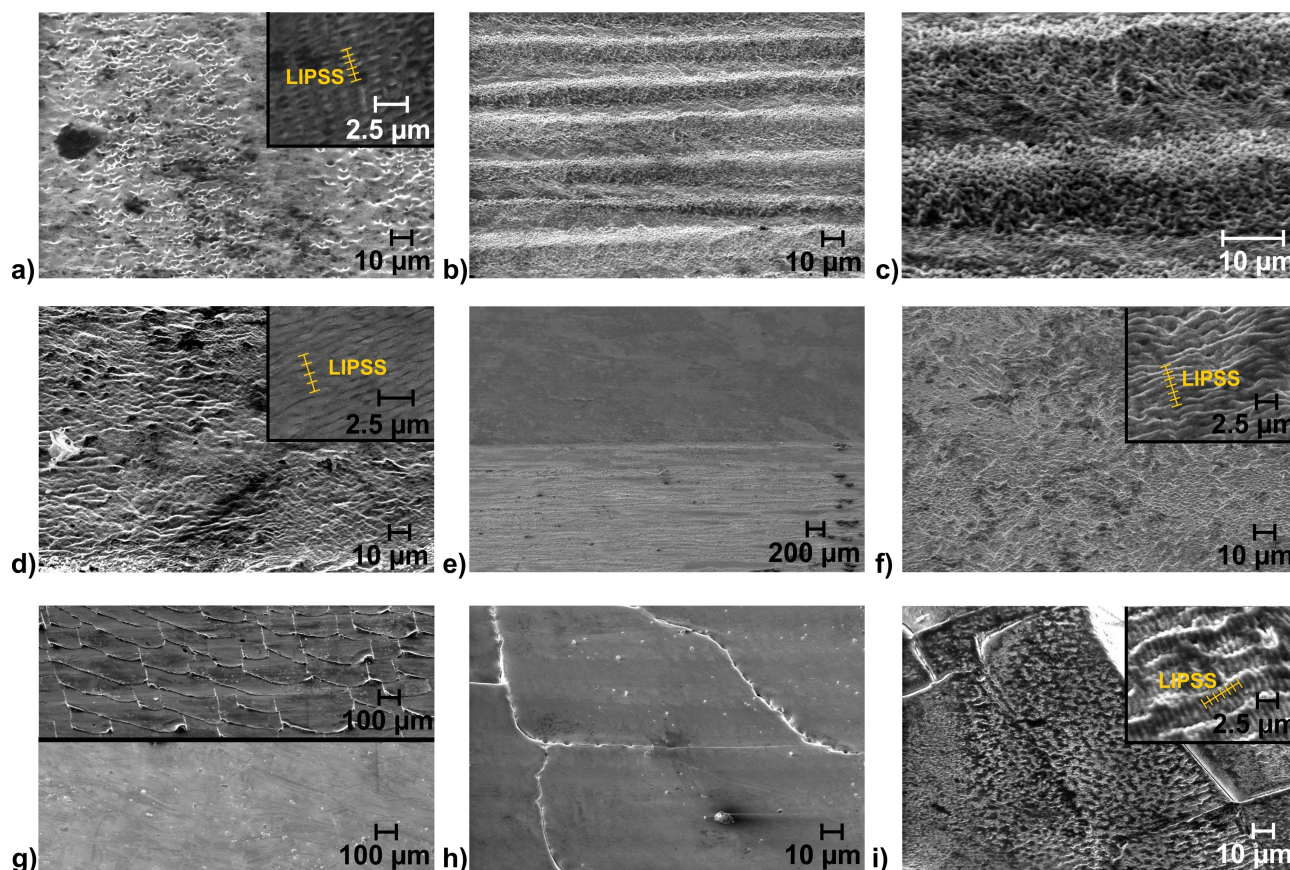


Figure 5. SEM images of titanium samples treated (a) in argon, (b,c) air, (d) nitrogen and (f) ethene/argon 60/40 atmosphere. (e) Sharp edge of the processed area (bottom) to the untreated Ti sample (top) under a nitrogen atmosphere. (g) Wide view of silicon sample untreated (bottom) and treated in argon (top). (h) Si treated in argon and (i) ethene/argon atmosphere.

down to a resolution of 0.5 nm are homogeneously transformed to TiC (Figure 6a). The SEM image (Figure 6b) visualizes the weak change in the surface structure, in contrast to the deep black appearance of the structured areas in the photographic image (Figure 6a).

To elucidate the chemical structure of the coating besides the elemental composition, the surfaces have been investigated by diffuse reflectance UV/VIS spectroscopy and surface X-ray diffraction (XRD). The UV/Vis spectra of the titanium sample processed under argon reveal a linear shift compared to the plane Ti surface (Figure 7a) as expected for a surface roughening without change of the chemical composition. The sample **Ti-air** shows an absorbance increasing from $\lambda=450$ nm to 800 nm, which matches with the dark blue color of the sample and the expectation of the formation of oxygen-deficient TiO₂. This is confirmed in the XRD pattern, which reveals a set of signals for TiO at $2\theta=36.9^\circ$ and 42.9° , underlying Ti and a broad signal corresponding to TiO₂ (rutile) at $2\theta=27.4^\circ$.^[59–61] The formation of anatase ($2\theta=25.3^\circ$) has not been identified.^[62] The signals for TiO are slightly shifted in comparison to the literature values of pure TiO. This can be explained by the nitrogen content of the sample processed at air as discussed above. The effect is much more pronounced in case of the titanium sample processed in a nitrogen atmosphere. The insert

of Figure 7d demonstrates the shift of the XRD peak positions, e.g. from 43.0° (pure TiO) to 42.9° (sample **Ti-air**) and further to 42.7° (sample **Ti-N**) and 42.6° (pure TiN^[63]). The exchange of oxygen in the crystal structure of TiO by larger nitrogen ions towards the isomorphous TiON/TiN (all NaCl type) leads to an increase of the lattice parameters and consequently the XRD peak positions shift to lower angles.^[4] The diffractogram confirms a layer of titanium oxynitride to be formed on the titanium sample processed under nitrogen and the peak positions match with a rough estimation of an N:O ratio of approx. 1:0.75 determined by EDX. The golden color of the titanium oxynitride coating is reflected by the broad absorbance peak around $\lambda=420$ nm in the diffuse reflectance spectra (Figure 7a). The peak position matches with the dip of the reflectance reported in literature for TiON films deposited by magnetron sputtering with an N:O ratio around 1:1.^[64]

The titanium sample processed in the ethene/argon atmosphere shows an intense absorption across the full spectrum (Figure 7a). The surface XRD measurements reveal two sets of signals, which are assigned to TiC and underlying Ti (Figure 7e).^[60,65] All peak positions of TiC are slightly shifted in comparison to the reference values given in literature. For example, the peak positions of pure TiC at $2\theta=36.0^\circ$, 41.8° and 60.65° are shifted to $2\theta=36.2^\circ$, 42.0° and 61.0° on the sample

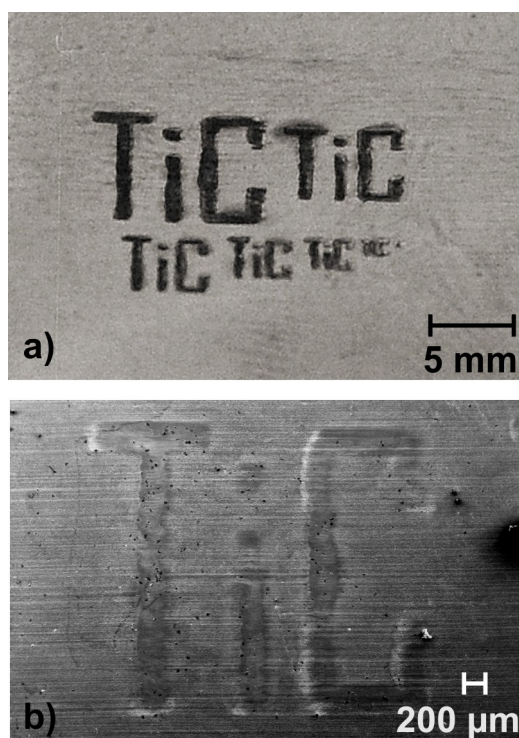


Figure 6. Spatial resolution of the high pulse repetition rate femtosecond laser carburizing process demonstrated by laser processing a vector image on Ti-6Al-4V in ethene/argon 60/40 atmosphere. (a) Photographic and (b) SEM image.

Ti-C. Again, this is explained by a partial exchange of carbon by oxygen in the cubic crystal lattice and the peak shift is in accordance with literature for the formation of titanium oxycarbides.^[66] According to the EDX measurements, the C:O ratio has been determined to roughly 1:0.25.

In contrast to the titanium samples, the diffractogram of the silicon sample processed in the ethene/air atmosphere reveals more intense reflections of the substrate. This might indicate a thinner carbide layer formed on silicon, although the larger attenuation length of the incident X-ray beam on silicon compared to titanium must be kept in mind, which leads to a larger amount of bulk material contributing to the observed spectrum. The carbon content determined by EDX is lower compared to the silicon sample, too (19.6 ± 2.0 atom-% C). Again, the larger penetration depth of the electron beam on the silicon substrate must be kept in mind. The most prominent signal of the diffractogram at $2\theta = 69.2^\circ$ is caused from Si (400) planes. Furthermore, the peak at 61.7° is caused from diffraction of Cu-K β radiation additionally emitted from the copper X-ray tube at the Si (400) plane.^[67] The forbidden reflection of Si (200) at $2\theta = 33^\circ$ has not been observed.^[67] Further weak peaks are assigned to the reflections at Si (111) around $2\theta = 29^\circ$ and Si (311) around $2\theta = 56^\circ$.^[25] The formation of β -SiC has been identified by the characteristic peak positions at $2\theta = 33.9^\circ$ and 35.8° (see insert of Figure 7e).^[25,68] The signal at $2\theta = 35.8^\circ$ is caused by diffraction at SiC (111) planes while the broader peak around $2\theta = 33.9^\circ$ is typical for planar defects of the (111) plane.^[68] The formation of cristobalite has not been observed,

which matches with the low oxygen content determined by EDX (Table 2). The diffractogram of the laser processed silicon surface in an ethene/argon atmosphere shows some similarity to the XRD pattern of SiC nanoparticles formed by laser ablation given in literature.^[25]

A microscopic view of the sample Si-C (see insert of Figure 7b) confirms the iridescent appearance on a black surface. The diffuse reflectance measurements of untreated Si as well as the sample laser processed under an argon atmosphere reveal nearly identical spectra (Figure 7b). The absorbance spectra reveal a clear dip around 365 nm (3.4 eV) which is in accordance with a peak of the reflectance of Si given in literature for undoped silicon and denoted as E_1 peak.^[52,69] After laser processing, the E_1 peak vanishes and the absorbance of the sample strongly increases, matching with the dark appearance of the surface. The deep black color of SiC is caused by small amounts of impurities, here possibly carbon (see below).

Since the signals detected by XRD were rather weak, the Si-C sample has additionally been investigated by surface Raman spectroscopy. The strong absorptivity of the black surface facilitates Raman excitation at $\lambda = 532$ nm. The Raman spectrum of Si-C reveals two intense peaks around $\tilde{\nu} = 500$ and 1000 cm^{-1} , which are assigned to silicon and are visible in the untreated sample, too (Figure 7c). Additionally, a peak around $\tilde{\nu} = 800$ cm^{-1} occurs after laser processing in the ethene/argon atmosphere. The peak is assigned to the transverse optical (TO) mode of SiC in accordance with literature.^[70] The longitudinal optical phonon mode of SiC around 970 cm^{-1} is covered by the 2TO peak of silicon (Figure 7c).^[70] Besides the Si and SiC signals, a weak broad peak around $\tilde{\nu} = 1350$ cm^{-1} was detected after laser processing, which corresponds to the D band of carbon (graphite) and reveals small amounts of carbon to be present, which is in accordance with the black color.^[70]

To gather further information about the surface structure, cross-sections of the samples Si-C and Ti-N were analyzed (Figure 8). A square has been cut out of the golden surface of the titanium sample processed under nitrogen (Ti-N) with a focused gallium ion beam (Figure 8b). The sample has been observed at a viewing angle of 35° with high resolution SEM to visualize the edge and an EDX scan has been performed beginning on top of the surface down to some micrometers into the material vertically along the cross section. The SEM images reveal the surface to be covered with a grainy microstructure based on homogeneously distributed small protrusions on the scale of some ten nanometers (Figure 8c). Interestingly, the surface layer is not covered with isolated particles, but the protrusions are seamlessly connected to the bulk material as visualized in Fig 8c showing the cross-section through several protrusions. Consequently, the surface layer may provide a good adhesion on the bulk material. The grainy layer itself revealed a nitrogen content of 17 atom-% N in agreement with the results discussed above. We were not able to detect nitrogen directly below the protrusions or deeper in the material. Although this might be seen as an indication for a very thin coating, the viewing-angle of the EDX analysis in combination with the penetration depth of the electron beam

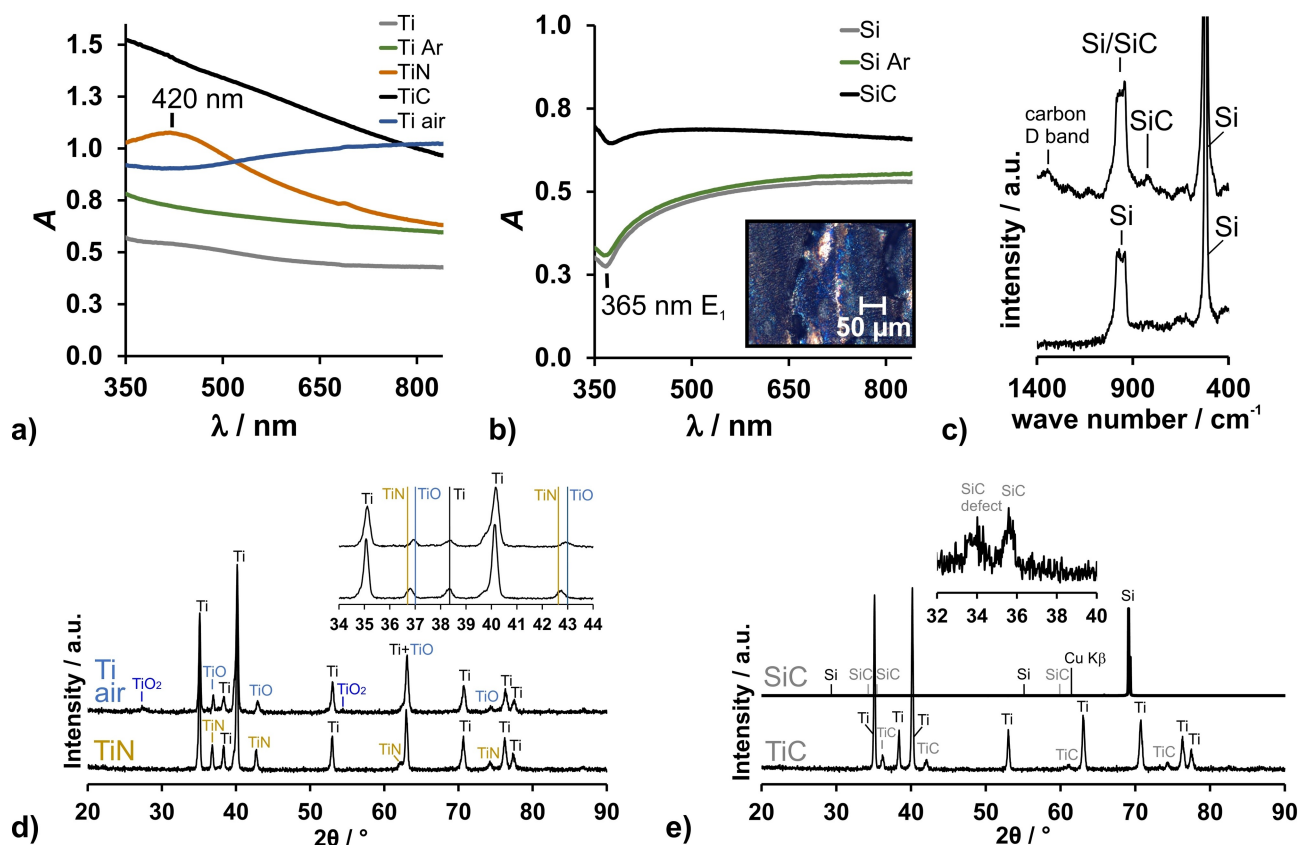


Figure 7. Diffuse reflectance spectra of (a) Ti (untreated, gray) processed under argon (green), air (blue), nitrogen (orange) and ethene/argon (black) atmosphere as well as (b) Si (untreated, gray) processed under argon (green) and ethene/argon (black) atmosphere (insert: optical micrograph of ethene/argon processed sample). (c) Surface Raman spectrum of plane silicon (bottom) and laser processed in an ethene/argon atmosphere (top). Surface X-ray diffraction patterns of (d) Ti processed under nitrogen (bottom) and air (top) (insert: excerpt from $2\theta = 34 - 44^\circ$, vertical lines represent exact values of pure TiN and TiO given in literature^[59,63]) and (e) Ti (bottom) and Si (top) processed under ethene/argon atmosphere.

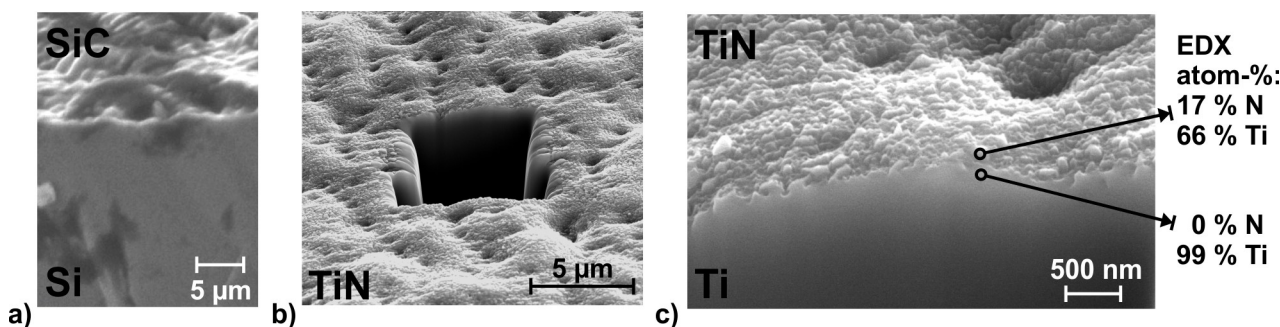


Figure 8. SEM image of cross section of (a) silicon processed under ethene/argon atmosphere and (b,c) SEM images of cross-section obtained by a focused ion beam of the titanium surface laser processed in a nitrogen atmosphere.

of approx. 1 μ m makes it difficult to quantify the results. Roughly, we can estimate the thickness of the nitride layer to be at least in the range of some ten nanometers as this is dimension of the grainy particular layer, but clearly below 1 μ m based on the EDX analysis of the cross-section. Basically the same result has been observed for a cross section of a silicon sample processed in ethene/argon atmosphere (Figure 8a and S2 of the Supporting Information). We were only able to detect carbon in the top layer (19.6 atom-% C) and not below.

To further investigate the stability of the surface coating, scratch testes have been performed. As discussed above, presented in literature and visualized in Figure 1, the micro-conical and porous surface layer obtained with a femtosecond laser setup with a repetition rate around 10 kHz is easily scratched off with a tip with a hardness below the bulk material.^[9,10,12] Treating the samples Ti-N, Ti-C and Si-C with a tip hard enough to scratch the bulk material reveals the coating to be hard enough to prevent the surface from being affected (Figure 9) An analysis of the depth profile via LSM reveals the

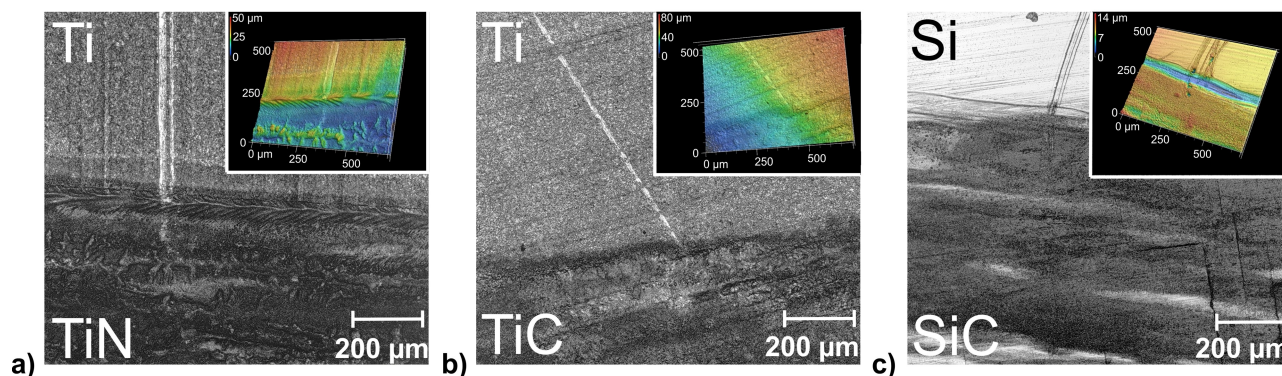


Figure 9. Optical microscopic images (insert: depth information from laser scanning microscopy) of scratches obtained with a hardness tip (on Ti: Mohs hardness 6, on Si: Mohs hardness 7) on the untreated and laser processed area of (a) titanium (processed under nitrogen), (b) titanium (processed under ethene/argon) and (c) silicon (processed under ethene/argon).

scratch on the bulk material with a depth of a few micrometers to be absent on the titanium oxynitride, oxycarbide or silicon carbide surface (Figure 9). The good adhesion of the surface layer can be explained by the high repetition rate of the laser process, favoring protrusions instead of particle ablation and redeposition as well as the process conditions based on gaseous nitrogen/carbon sources instead of liquids which promote rapid cooling and particle formation.

Conclusion

Coatings based on TiN/TiON, TiC/TiOC and SiC are of interest for various applications, ranging from hardened tools to biocompatible surfaces. Typically, chemical processes (often induced by a plasma) or physical (sputtering)/chemical vapor deposition techniques are applied. The methods generate highly stable, flat surfaces covering the whole workpiece with a thickness of some micrometers. A completely different surface is obtained with low repetition rate femtosecond laser structuring processes in the presence of nitrogen/carbon sources. In these cases, the surface structure is a major aspect and the often microconical, porous structural motif is prone to mechanical damage. The femtosecond laser coating process based on high power high repetition rate laser systems in the presence of gaseous sources for carbon or nitrogen discussed here is located at the gap between laser structuring with femtosecond lasers and common carburizing/nitriding techniques. On the one hand, the surfaces are clearly less structured than the characteristic motifs from low repetition rate femtosecond lasers, but significantly more robust and on the other hand they are clearly thinner and not as even as surfaces obtained by chemical/physical deposition processes, but provide a unique surface structure and surfaces can be coated spatially resolved. The process presented here is fast, with a process time of a few seconds per square centimeter and provides a high spatial resolution below 0.5 mm at the same time. The chemical surface composition has been investigated by EDX and a nitrogen content up to 20 atom-% N and a carbon content up to 30 atom-% C is achieved, while XRD confirms the formation

of TiN (TiON), TiC (TiOC) and SiC. The carburizing process has been optimized by using ethene instead of methane as process gas atmosphere and diluting the ethene by argon to prevent overwhelming carbon release. The high power high pulse repetition rate carburizing/nitriding process is not competitive for surface hardening of full workpieces, but can provide a single step opportunity to deliver a roughened/LIPSS coated and chemically transformed surface. Such surfaces are of interest e.g. in terms of their biocompatibility.^[16,18] Currently, titanium surfaces presented here are under investigation concerning their potential as electrode coating and controlling surface wettability.

Experimental Section

Caution! Laser irradiation in acetylene atmospheres can initiate explosions. Careful control of the gas mixture is required.

Plates of titanium (99.6 + %) with 1 mm thickness and Ti-6Al-4V with 0.5 mm thickness have been obtained from *Goodfellow*. Silicon wafer chips (0.5 mm thickness) were kindly provided by the Institute of Polymer Materials and Plastics Engineering of the Clausthal University of Technology. Substrates have been cleaned by ultrasonication with acetone and deionized water. Argon, nitrogen, oxygen, ethene (*Linde*) and acetylene (*air liquide*) have been used as received. Diffuse reflectance UV/Vis Spectra have been recorded with a *Jasco V650* spectrophotometer equipped with an integrating sphere (*Jasco ISV-722*). Spectra are referenced to a standard white sample given by the supplier (reflectivity $\rho = 1$) and absorbance spectra have been calculated according to $A = \log(\rho^{-1})$. Scratch tests have been performed with a standardized hardness scale test kit (*Krantz I 170*) under a constant load of 0.05 N. The end tip diameter of the conical scratch tips was 20 μm . Tips of apatite (Mohs hardness 5), feldspar (hardness 6) and quartz (hardness 7) have been used. Scanning electron microscopy (SEM) images have been taken with an EVO MA10 (*Zeiss*) SEM operated at 10 kV. Elemental composition of surfaces has been determined with an integrated energy dispersive X-ray spectroscopy (EDX) unit (*Bruker XFlash 6/30*) at 10 kV. For the elemental composition of surfaces, areas of $1000 \times 1000 \mu\text{m}^2$ have been analyzed. The penetration depth of the incident electron beam is assumed to approx. 1 μm (0.9 μm on Ti, 1.5 μm on Si). Surface roughness and depth information have been measured and visualized with a laser scanning microscope (LSM) operated at 408 nm (*Keyence VK-X200*).

For a crystallographic analysis of the sample surface, XRD measurements were performed using an X-ray diffractometer (Empyrean, Malvern Panalytical Ltd.) equipped with a copper X-ray tube (Cu-K α , $\lambda = 1.5406 \text{ \AA}$). The penetration depth of the incident X-ray beam is assumed to approx. 2–7 μm on Ti and 12–50 μm on Si depending on the angle of the incident beam. Surface Raman spectra have been measured with a Raman microscope (Bruker Senterra) in a backscattering geometry with an excitation wavelength of $\lambda = 532 \text{ nm}$ at 20 mW and a laser spot size with a diameter of 1.6 μm . Focused Ion Beam (FIB) cross-sections and field emission SEM imaging have been performed by the Clausthal Centre for Material Technology (CZM). EDX scans have been performed to analyze the cross section in segments of $30 \times 30 \text{ nm}^2$.

For comparison, titanium samples have been processed with a Ti:sapphire laser source ($\lambda = 800 \text{ nm}$) with $\tau = 60 \text{ fs}$ laser pulses at a repetition rate of $f = 10 \text{ kHz}$ according to a setup reported previously.^[71]

The general setup for laser surface processing used here has been described earlier.^[72,73] An AMPHOS 400 Yb:YAG high power laser system with a centre wavelength of $\lambda = 1030 \text{ nm}$ and a pulse length of $\tau = 750 \text{ ns}$ has been used as beam source. The direction of polarization of the linearly polarized light correlated with the scanning direction. Besides the preliminary parameter variation, the following parameters have been used for all final samples at varying gas atmospheres. A spot diameter of the Gaussian beam of approximately $S = 140 \mu\text{m}$ ($1/e^2$) has been adjusted by a 420 mm f-theta objective. The average optical laser output power of $P = 95 \text{ W}$ (Si: 76 W) leads to a pulse energy of $E = 95 \mu\text{J}$ (Si: 76 μJ) and a laser fluence of $J = 0.62 \text{ J/cm}^2$ (Si: 0.50 J/cm^2) at a repetition rate of $f = 1 \text{ MHz}$. The scanning speed of $v = 560 \text{ mm/s}$ of the laser beam on the surface results in every spot on the surface to be hit by a number of $N = 250$ laser pulses. Areas of $1 \times 1 \text{ cm}^2$ (parameter variation) and $2 \times 2 \text{ cm}^2$ (final samples) have been processed in lines with a line distance of $D = 60 \mu\text{m}$. All experiments have been performed within an air-tight stainless steel processing chamber (inner diameter 10 cm) equipped with an NIR transparent window, 2 inlet and outlet valves and oxygen and pressure sensors. The total volume of the chamber is 0.65 L. The inner atmosphere of the chamber has been exchanged by repeated evacuation and flushing with the desired gas atmosphere. All samples have been cleaned by ultrasonication in deionized water for 5 min. Samples have been stored at ambient conditions.

Acknowledgements

We gratefully acknowledge financial support from the German Federal Ministry of Education and Research (BMBF) within the context of the project ZiLSicher (03XP0191F). We sincerely thank Karin Bode from the Institute of Inorganic and Analytical Chemistry of the Clausthal University of Technology for Raman surface measurements (Raman microscope is funded by the Deutsche Forschungsgemeinschaft (DFG, German Research Foundation) - INST 189/172-1 FUGG), Simon Rauh for help with the gas mixing setup and Thomas Gimpel (Clausthal University of Technology, Research Center for Energy Storage Technologies) for access to the Ti:sapphire laser setup. Open access funding enabled and organized by Projekt DEAL.

Conflict of Interest

The authors declare no conflict of interest.

Keywords: carbides · femtosecond lasers · nitrides · surface modification · titanium

- [1] A. Gupta, D. Paramanik, S. Varma, C. Jacob, *Bull. Mater. Sci.* **2004**, *27*, 445–451.
- [2] F. M. El-Hossary, N. Z. Negm, A. M. Abd El-Rahman, M. Raaf, A. A. Abd Elmula, *Adv. Chem. Engineer. Sci.* **2015**, *5*, 1–14.
- [3] J.-M. Chappé, N. Martin, J. Lintymer, F. Sthal, G. Terwagne, J. Takadom, *Appl. Surf. Sci.* **2007**, *253*, 5312–5316.
- [4] O. Banakh, M. Moussa, J. Matthey, A. Pontearso, M. Cattani-Lorente, R. Sanjines, P. Fontana, A. Wiskott, S. Durual, *Appl. Surf. Sci.* **2014**, *317*, 986–993.
- [5] B. Subramanian, C. V. Muraleedharan, R. Ananthakumar, M. Jayachandran, *Surf. Coat. Technol.* **2011**, *205*, 5014–5020.
- [6] S. Windecker, I. Mayer, G. De Pasquale, W. Maier, O. Dirsch, P. De Groot, Y.-P. Wu, G. Noll, B. Leskosek, B. Meier, O. M. Hess, *Circulation* **2001**, *104*, 928–933.
- [7] N. Martin, R. Sanjines, J. Takadom, F. Lévy, *Surf. Coat. Technol.* **2001**, *142–144*, 615–620.
- [8] R. Dhiman, P. Morgen, *Thin Solid Films* **2013**, *536*, 130–135.
- [9] P. Schaaf, E. Carpena, M. Kahle, M. Han, *Adv. In Solid State Phys.* vol. 42 (Ed.: B. Kramer), Springer, Berlin, 2002, pp. 219–231.
- [10] P. Schaaf, *Proc. SPIE* **2003**, *5147*, 404–415.
- [11] E. Carpena, P. Schaaf, M. Han, K. P. Lieb, M. Shinn, *Appl. Surf. Sci.* **2002**, *186*, 195–199.
- [12] D. Höche, P. Schaaf, *Heat Mass Transf.* **2011**, *47*, 519–540.
- [13] A. Y. Vorobyev, C. Guo, *Laser Photonics Rev.* **2013**, *7*, 385–407.
- [14] K. Sugioka, Y. Cheng, *Light-Sci. Appl.* **2014**, *3*, e149.
- [15] G. Dumitru, V. Romano, H. P. Weber, M. Sentis, W. Marine, *Appl. Phys. A* **2002**, *74*, 729–739.
- [16] M. Y. Gazizova, N. A. Smirnov, S. I. Kudrayshov, V. V. Shugurov, *Iop. Conf. Ser. Mater. Sci. Eng.* **2020**, *862*, 022054.
- [17] Z. Zhai, C. Wei, Y. Zhang, Y. Cui, Q. Zeng, *Appl. Surf. Sci.* **2020**, *502*, 144131.
- [18] M. K. Kuntumalla, V. V. S. S. Srikanth, *Mater. Lett.* **2019**, *243*, 136–139.
- [19] B. Meng, J. Zheng, D. Yuan, S. Xu, *Appl. Phys. A* **2019**, *125*, 69.
- [20] J. Bonse, S. V. Kirner, R. Koter, S. Pentzien, D. Spaltmann, J. Krüger, *Appl. Surf. Sci.* **2017**, *418*, 572–579.
- [21] G. Dumitru, V. Romano, Y. Gerbig, H. P. Weber, H. Haefke, *Appl. Phys. A* **2005**, *80*, 283–287.
- [22] L. Gemini, M. Hashida, M. Shimizu, Y. Miyasaka, S. Inoue, S. Tokita, J. Limpouch, T. Mocek, S. Sakabe, *J. Appl. Phys.* **2013**, *114*, 194903.
- [23] J. E. Krzanowski, R. E. Leuchtner, *J. Am. Ceram. Soc.* **1997**, *80*, 1277–1280.
- [24] M. Vendan, P. Molian, A. Bastawros, J. Anderegg, *Mater. Sci. Semicond. Process.* **2005**, *8*, 630–645.
- [25] X. Yu, S. Terakawa, S. Hayashi, T. Asaka, F. Itoigawa, S. Ono, J. Takayanagi, *Arabian J. Sci. Eng.* **2017**, *42*, 4221–4226.
- [26] P. G. Kuzmin, G. A. Shafeev, V. V. Bukin, S. V. Garnov, C. Farcau, R. Carles, B. Warot-Fontrose, V. Guieu, G. Viau, *J. Phys. Chem. C* **2010**, *114*, 15266–15273.
- [27] A. V. Ivashchenko, D. A. Kochuev, K. S. Khorkov, V. G. Prokoshev, M. A. Tarasova, *J. Phys. Conf. Ser.* **2019**, *1238*, 012033.
- [28] G. Leggeri, A. Luches, A. Perrone, G. Majni, P. Mengucci, *Vacuum* **1995**, *46*, 991–995.
- [29] Z. Zhang, P. A. VanRompay, J. A. Nees, R. Clarke, X. Pan, P. P. Pronko, *Appl. Surf. Sci.* **2000**, *154–155*, 165–171.
- [30] S. Tóth, P. Németh, P. Rácz, L. Himics, P. Dombi, M. Koós, *Diamond Relat. Mater.* **2018**, *81*, 96–102.
- [31] D. A. Kochuev, K. S. Khorkov, D. V. Abramov, S. M. Arakelian, V. G. Prokoshev, *J. Surf. Invest. X-ray, Synchrotron Neutron Tech.* **2018**, *12*, 1220–1223.
- [32] A. Ivashchenko, D. Kochuev, N. Davydov, *Solid State Phenom.* **2020**, *299*, 743–748.
- [33] D. Zhang, B. Ranjan, T. Tanaka, K. Sugioka, *ACS Appl. Nano Mater.* **2020**, *3*, 1855–1871.
- [34] J. Lehr, F. de Marchi, L. Matus, J. MacLeod, F. Rosei, A.-M. Kietzig, *Appl. Surf. Sci.* **2014**, *320*, 455–465.

- [35] S. Hammouti, B. Holybee, W. Zhu, J. P. Allain, B. Jurczyk, D. N. Ruzic, *Appl. Phys. A* **2018**, *124*, 411.
- [36] K. Wöbbeking, M. Li, E. G. Hübner, W. Schade, *RSC Adv.* **2019**, *9*, 37598–37607.
- [37] B. K. Nayak, M. C. Gupta, *Opt. Lasers Eng.* **2010**, *48*, 940–949.
- [38] B. K. Nayak, M. C. Gupta, *Opt. Lasers Eng.* **2010**, *48*, 966–973.
- [39] J. Schille, L. Schneider, A. Streek, S. Kloetzer, U. Loeschner, *Opt. Eng.* **2016**, *55*, 096109.
- [40] J. Finger, C. Kalupka, M. Reininghaus, *J. Mater. Process. Technol.* **2015**, *226*, 221–227.
- [41] *CRC Handbook of Chemistry and Physics*, 84th edition (Ed.: D. R. Lide), CRC Press LLC, Boca Raton, **2004**.
- [42] *Handbook of the Physicochemical Properties of the Elements*, 1st edition (Ed.: G. V. Samsonov), IFI / Plenum, New York, **1968**.
- [43] D. Tabor, *The hardness of metals* (Ed. W. Jackson, H. Fröhlich, N. F. Mott), Oxford University Press, London, **1951**.
- [44] M. Boivineau, C. Cagran, D. Doytier, V. Eyraud, M.-H. Nadal, B. Wilthan, G. Pottlacher, *Int. J. Thermophys.* **2006**, *27*, 507–529.
- [45] *Gmelin Handbook of Inorganic Chemistry – Titan*, 8th edition (Ed. R. J. Meyer, E. H. E. Pietsch), Springer, Berlin, **1951**.
- [46] A. F. Holleman, E. Wiberg, N. Wiberg, G. Fischer, *Lehrbuch der Anorganischen Chemie*, 102nd edition, de Gruyter, Berlin, **2007**.
- [47] *Römpf Chemie Lexikon*, 9th edition (Ed.: J. Falbe, M. Regitz), Georg Thieme, Stuttgart, **1995**.
- [48] A. Heintz, *Thermodynamik der Mischungen*, 1st edition, Springer, Berlin, **2017**.
- [49] D. Steinborn, *Grundlagen der metallorganischen Komplexkatalyse*, 2nd edition, Springer, Berlin, **2010**.
- [50] D. L. Vrel, J.-M. Lihmann, J.-P. Petitot, *J. Chem. Eng. Data* **1995**, *40*, 280–282.
- [51] P. Mannion, J. Magee, E. Coyne, G. M. O'Connor, *Proc SPIE* **2003**, *4876*, 470–478.
- [52] M. A. Green, M. J. Keevers, *Prog. Photovolt: Res. Appl.* **1995**, *3*, 189–192.
- [53] J. Thorstensen, S. E. Foss, *J. Appl. Phys.* **2012**, *112*, 103514.
- [54] S. Rauh, K. Wöbbeking, M. Li, W. Schade, E. G. Hübner, *ChemPhysChem* **2020**, *21*, 1644–1652.
- [55] A. Reau, B. Guizard, C. Mengeot, L. Boulanger, F. Ténégal, *Mater. Sci. Forum* **2007**, *534–536*, 85–88.
- [56] B. Zhang, N. Mehrjoo, H. D. Ng, J. H. S. Lee, C. Bai, *Combust. Flame* **2014**, *161*, 1390–1397.
- [57] I. Gnilitzkiy, T. J.-Y. Derrien, Y. Levy, N. M. Bulgakova, T. Mocek, L. Orazi, *Sci. Rep.* **2017**, *7*, 8485.
- [58] C. Zhang, L. Cheng, B. Tan, Z. Chen, W. Zhang, Z. Liu, J. Peng, *Microsyst. Technol.* **2020**, *26*, 2767–2776.
- [59] S. Bartkowski, M. Neumann, E. Z. Kurmaev, V. V. Fedorenko, S. N. Shamin, V. M. Cherkashenko, S. N. Nemnonov, A. Winiarski, D. C. Rubie, *Phys. Rev. B* **1997**, *56*, 10656–10667.
- [60] N. Schmitz-Pranghe, P. Dünner, *Z. Metallkd.* **1968**, *59*, 377–382.
- [61] E. P. Meagher, G. A. Lager, *Canad. Mineral.* **1979**, *17*, 77–85.
- [62] M. Horn, C. F. Schwerdtfeger, E. P. Meagher, *Z. Kristallogr. – Cryst. Mater.* **1972**, *136*, 273–281.
- [63] S. I. Alyamovskii, B. V. Mitrofanov, Y. G. Zainulin, G. P. Shveikin, *Teplofiz. Vys. Temp.* **1973**, *11*, 680–682.
- [64] F. Chen, S.-W. Wang, L. Yu, X. Chen, W. Lu, *Opt. Mater. Express* **2014**, *4*, 1833–1847.
- [65] W. Hofmann, A. Schrader, *Arch. Eisenhuettenwes.* **1936**, *10*, 65–66.
- [66] D. N. Miller, A. K. Azad, H. Delpouve, L. Quazuguel, J. Zhou, A. Sinha, P. Wormald, J. T. S. Irvine, *J. Mater. Chem. A* **2016**, *4*, 5730–5736.
- [67] A. Gupta, D. Paramanik, S. Varma, C. Jacob, *Bull. Mater. Sci.* **2004**, *27*, 445–451.
- [68] H. Cui, Y. Zheng, J. Ma, S. Yang, G. Tian, L. Shang, X. Liu, *J. Wood Sci.* **2017**, *63*, 95–103.
- [69] B. Lojek, 11th IEEE International Conference on Advanced Thermal Processing of Semiconductors **2003**, Charleston, SC, USA. Conference proceeding, 215–220. DOI: 10.1109/RTP.2003.1249151.
- [70] C. Wang, N. Huang, H. Zhuang, Z. Zhai, B. Yang, L. Liu, X. Jiang, *Surf. Coat. Technol.* **2016**, *299*, 96–103.
- [71] A. Gabler, C. I. Müller, T. Rauscher, T. Gimpel, R. Hahn, M. Köhring, B. Kieback, L. Röntzsch, W. Schade, *Int. J. Hydrogen Energy* **2018**, *43*, 7216–7226.
- [72] K. Wöbbeking, M. Li, W. Schade, E. G. Hübner, *J. Phys. Commun.* **2020**, *4*, 111001.
- [73] S. B. Beil, T. Müller, S. B. Sillart, P. Franzmann, A. Bomm, M. Holtkamp, U. Karst, W. Schade, S. R. Waldvogel, *Angew. Chem.* **2018**, *130*, 2475–2479; *Angew. Chem. Int. Ed.* **2018**, *57*, 2450–2454.

Manuscript received: March 8, 2021
Revised manuscript received: April 16, 2021
Accepted manuscript online: April 19, 2021